ISSN 1990-7931, Russian Journal of Physical Chemistry B, 2016, Vol. 10, No. 1, pp. 91–99. © Pleiades Publishing, Ltd., 2016.
Original Russian Text © V.V. Klimenko, A.T. Karpachev, M.V. Klimenko, K.G. Ratovskii, N.A. Korenkova, 2016, published in Khimicheskaya Fizika, 2016, Vol. 35, No. 1, pp. 21–30.

CHEMICAL PHYSICS OF ATMOSPHERIC PHENOMENA

Latitudinal Structure of the Longitudinal Effect in the Nighttime Ionosphere during the Summer and Winter Solstice

V. V. Klimenko[a, *], A. T. Karpachev[b], M. V. Klimenko[a, c], K. G. Ratovskii[d], and N. A. Korenkova[a]

[a] *Western Branch of the Pushkov Institute of Terrestrial Magnetism, Ionosphere and Radio Wave Propagation, Russian Academy of Sciences, Kaliningrad, Russia*

[b] *Pushkov Institute of Terrestrial Magnetism, Ionosphere, and Radio Wave Propagation, Russian Academy of Sciences, Moscow, Russia*

[c] *Kant Baltic Federal University, Kaliningrad, Russia*

[d] *Institute Solar-Terrestrial Physics, Siberian Branch, Russian Academy of Sciences, Irkutsk, Russia*

**e-mail: vvk_48@mail.ru*

Received March 17, 2015

Abstract—The paper reports the basic morphological characteristics of the longitudinal variations of the electron density in the nighttime F region of the ionosphere at different latitudes obtained from data collected by the Intercosmos-19 satellite and from the results of calculations within the framework of the Global Self-Consistent Model of the Thermosphere, Ionosphere, and Protonosphere (GSM TIP). Based on the Intercosmos-19 satellite data for a high solar activity, spatial distributions of the critical frequency *fo*F2 of the F2 layer for near-midnight hours of the local time are plotted. The study revealed the main features of the mechanisms of the formation of longitudinal features of the nighttime ionosphere at various latitudes during the summer and winter solstices, as well as two reasons for their occurrence. In particular, we consider (1) the mechanisms of the formation of the nighttime peaks at the longitudes of the Yakutsk anomaly and Weddell Sea anomaly, (2) manifestations of longitudinal variations of the main ionospheric trough, and (3) the longitudinal dependence of the disappearance of the equatorial anomaly during the June and December solstices.

Keywords: F-region of the ionosphere, longitudinal variations, Weddell Sea anomaly, Yakutsk anomaly, equatorial anomaly, electron density, numerical simulation, Intercosmos-19, ionosonde

DOI: 10.1134/S1990793116010073

1. INTRODUCTION

One of the most important properties of the Earth's ionosphere is its longitudinal variability, since longitudinal variations of the ionospheric parameters are comparable in magnitude with the diurnal variations, a factor important for the prediction of radio wave propagation in calm conditions and during geomagnetic disturbances. Longitudinal variations of parameters of the F2 layer of the ionosphere over the entire range of longitudes were first identified by researchers from the Pushkov Institute of Terrestrial Magnetism, Ionosphere, and Radio Wave Propagation of the Russian Academy of Sciences (IZMIRRAN) based on data from the Intercosmos-19 (IC-19) satellite [1, 2]. The most striking manifestations of longitudinal variations in the ionosphere are the Weddell Sea anomaly [3] and the Yakutsk anomaly [4], which arise in a certain range of longitudes, which makes it possible to interpret them in terms of longitudinal anomalies. Note that researchers of these anomalies most often point to abnormally high summer nighttime values of the electron density at the longitudes of Yakutsk and the Weddell Sea [5–7]. Nighttime longitudinal variations of the main ionospheric trough, mid-latitude nighttime maximum, and equatorial anomaly (EA) have been studied for many years at IZMIRAN based on measurements by different satellites [8–18]. Note that the measurement data from the IC-19 satellite were among the first to be used in studying the nighttime longitudinal variations of the electron density in the ionosphere on a global scale. This allowed researchers from IZMIRAN to identify a four-wave structure in the longitudinal variation of the electron density at low latitudes long before its existence was commonly accepted.

Despite the fact that the main morphological features and mechanisms of the formation of these large-scale inhomogeneities are fairly well known, until now there had been no detailed comparative analysis of longitudinal variations of the electron density in the equatorial, low-latitude, mid-latitude, sub-auroral, and high-latitude ionosphere because of the scarcity of ionospheric data. Even the IRI empirical model, standardized in recent years, cannot describe these variations in the high- and low-latitude ionosphere. This suggests that, at present, the most effective

method for studying nighttime longitudinal variations of the ionospheric parameters is to use a numerical model of the ionosphere. Currently, there are a number of models of the ionosphere developed by different groups in our country under the leadership of V.S. Mingalev (Polar Geophysical Institute, Kola Scientific Center, RAS) [19], V.M. Uvarov (Arctic and Antarctic Research Institute) [20], A.V. Pavlov (Pushkov Institute of Terrestrial Magnetism, Ionosphere, and Radio Wave Propagation RAS) [21], A.V. Tashchilin (Institute of Solar–Terrestrial Physics, SB RAS) [22], as well as groups by abroad: TDIM (Time-Dependent Ionospheric Model), USA [23]; SUPIM (Sheffield University Plasmasphere Ionosphere Model), England [24]; SAMI2 and SAMI3 (Sami is Another Model of the Ionosphere), USA [25, 26]. In all of these models, various characteristics of the near-Earth medium, such the conductivity of the ionosphere, electric field, composition, thermal mode, and dynamics of the neutral atmosphere, are input parameters, which are specified based on calculations by empirical models. In contrast to the aforementioned models, in a variety of models, such as the GSM TIP (Global Self-Consistent Model of the Thermosphere, Ionosphere, Protonosphere), Kaliningrad [27–29]; UAM (Upper Atmosphere Model), Murmansk [30]; TIME GCM (Thermosphere–Ionosphere–Mesosphere–Electrodynamics General Circulation Model), USA [31]; CTIPE (Coupled Thermosphere Ionosphere Plasmasphere Electrodynamics model), England, USA [32]; GAIA (Whole Atmosphere-Ionosphere Coupled Model), Japan [33], the structure, thermal conditions, and dynamics of the neutral atmosphere and ionosphere, conductivity of the ionosphere, and electric field are calculated self-consistently. Note that the TIME GCM does not consider the horizontal transport of charged ionospheric plasma components, which makes the ionospheric block of this model not quite correct. A distinctive feature of the GSM TIP, UAM and CTIPe model is a self-consistent description of the plasmaspheric parameters and of the electric field of ionospheric and magnetospheric origin. The last modifications of the GSM TIP make it possible to correctly describe the distributions of the electric field and the electron density in the ionosphere at equatorial, middle, and high latitudes.

The earlier studies [33, 34], based on observational data from the IC-19 satellite and GSM TIP calculations, have demonstrated significant advantages of such association for studying various features of the ionosphere, including nighttime longitudinal variations at subauroral latitudes [35]. The purpose of the present work is to identify similarities and differences between longitudinal structures and mechanisms of their formation at different latitudes. As an additional database, we used information obtained by ground-based probing of the ionosphere in Irkutsk and Kaliningrad.

2. LONGITUDINAL VARIATIONS OF THE CRITICAL FREQUENCY *fo*F2 OF THE F2 LAYER IN THE NORTHERN AND SOUTHERN SUMMER HEMISPHERES IN THE NIGHTTIME ACCORDING TO IC-19 SATELLITE DATA AND GROUND-BASED PROBING

The IC-19 satellite operated in a period of high solar activity ($F_{10.7} = 150–250$), from February 1979 to March 1981. The satellite data, collected during more than 2000 orbit passes, cover all seasons and hours of local time. The satellite moved in an elliptical orbit at altitudes 500–1000 km with an inclination of 74°. External-probe ionograms were recorded on-board in a digital form at any longitude within the satellite orbit. In this study, we used the data received from the IC-19 satellite during the solstices in 1979 and 1980 in quiet geomagnetic conditions ($K_p \leqslant 3$). The measurement data are uniformly spread in longitude and local time, so that a 2-h LT interval, for which LT the maps were drawn, comprises from 2000 to 3500 *fo*F2 values. This makes it possible to construct an adequate longitude–latitude *fo*F2 distribution for the northern and southern hemispheres, which reflects the average conditions during the solstice.

Figure 1 shows the *fo*F2 maps in the longitude–dipole inclination coordinates for 23:00 LT, 00:00 LT, 02:00 LT and 04:00 LT drawn according to the IC-19 satellite data collected in June and December 1979. According to the IC-19 data, in the summer, at 23:00 LT, 00:00 LT, and 02:00 LT, a three-wave structure of longitudinal variations of *fo*F2 is formed in the crests and depression of the well-pronounced nighttime EA. (The $I = \pm 30°$ dipole inclination of the EA crests corresponds to a dipole latitudes of $\pm 17°$.) At 04:00 LT, the longitudinal variation of *fo*F2 in the region of the nighttime equatorial anomaly exhibits a two-wave structure, while the EA itself practically disappears. In the southern (winter) hemisphere, the longitudinal variation of the main ionospheric trough appears as a single-wave structure. At the longitude of 135° E in the northern (summer) hemisphere is seen the equatorial part of the Yakutsk anomaly: a maximum of in the nighttime longitudinal distribution of *fo*F2, the magnitude of which exceeds that in the daytime [35]. In addition, in the northern hemisphere at the mid- and subauroral latitudes, the formation of a longitudinal *fo*F2 variation in the form of a two-wave structure is observed.

In the winter northern hemisphere, at 23:00 LT and 00:00 LT, three- and four-wave structures of longitudinal *fo*F2 variations in the crests and depression of the nighttime equatorial anomaly. At 02:00 LT, the equatorial anomaly appears only at longitudes of Eurasia, whereas at 04:00 LT, the equatorial anomaly in *fo*F2 disappears at all longitudes. In all presented LT maps, the range of longitudes from 270° E to 285° E in the southern (summer) hemisphere clearly shows a

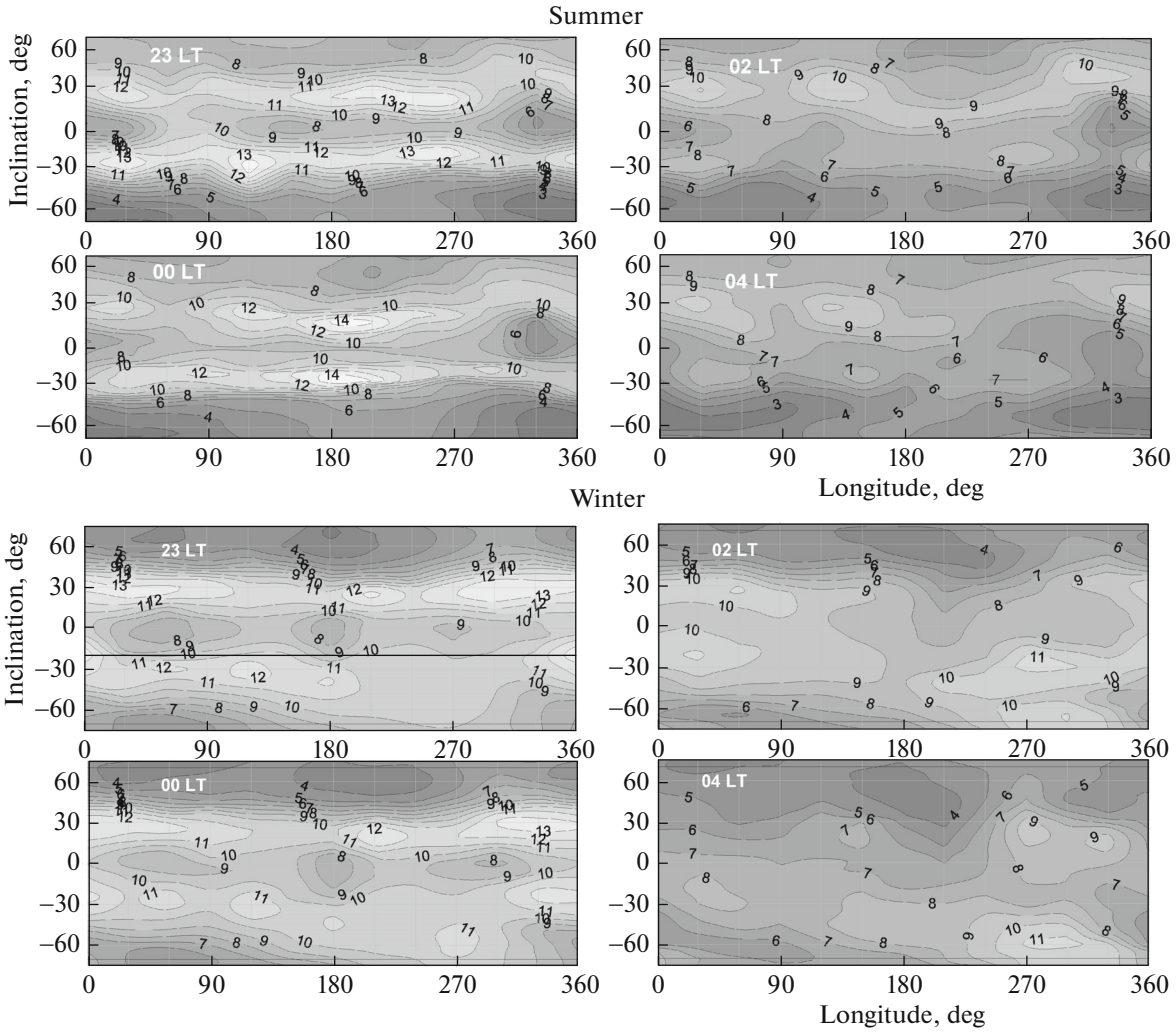

Fig. 1. Maps of the *fo*F2 distribution in the longitude–dipole inclination coordinates at 23:00, 00:00, 02:00, and 04:00 LT June (top) and December (bottom) 1979 drawn based on data from the Intercosmos-19 satellite.

maximum of the Weddell Sea anomaly near 60° S. At 02:00 LT and 04:00 LT, one can be clearly identify mid-latitude and sub-auroral maxima in the longitudinal variation of *fo*F2 in the American sector. This result indicates the absence of a connection (reported in [36]) between the EA crest and the nighttime maximum of the Weddell Sea anomaly. As for the longitudinal variation of the main ionospheric trough in the winter northern hemisphere, here, in contrast to the winter southern hemisphere, the longitudinal variation of *fo*F2 is formed as a two-wave structure with a less pronounced depression in Yakutsk and the North American longitudinal sectors. Note that the longitudinal variation is least pronounced in the mid-latitudes (~45° N).

A comparison of winter and summer conditions in the southern and northern hemispheres shows that the longitudinal variation of the equatorial anomaly in winter and summer has quite a complex structure with maxima in different longitudinal sectors. In this case, the longitudinal EA variations with four, three, two, and one-wave structures can exist. In certain hours of the local time, the longitudinal maxima are more pronounced in the northern crests, whereas in the other hours, in the southern. An inspection of nighttime longitudinal variations at the mid- and subauroral latitudes reveals a clear-cut morphology: (1) in the southern hemisphere, in winter and summer, a one-wave structure of the longitudinal variation is formed, especially at the latitudes of the main ionospheric trough (MIT) and the Weddell Sea anomaly; (2) two- and three-wave structures of the longitudinal variation are formed in the northern hemisphere, particularly pronounced at the latitudes of the winter MIT and Yakutsk anomaly; (3) in contrast to the southern hemisphere, where the longitudinal structures at the middle and auroral latitudes are identical, in the northern hemisphere, there is a significant difference

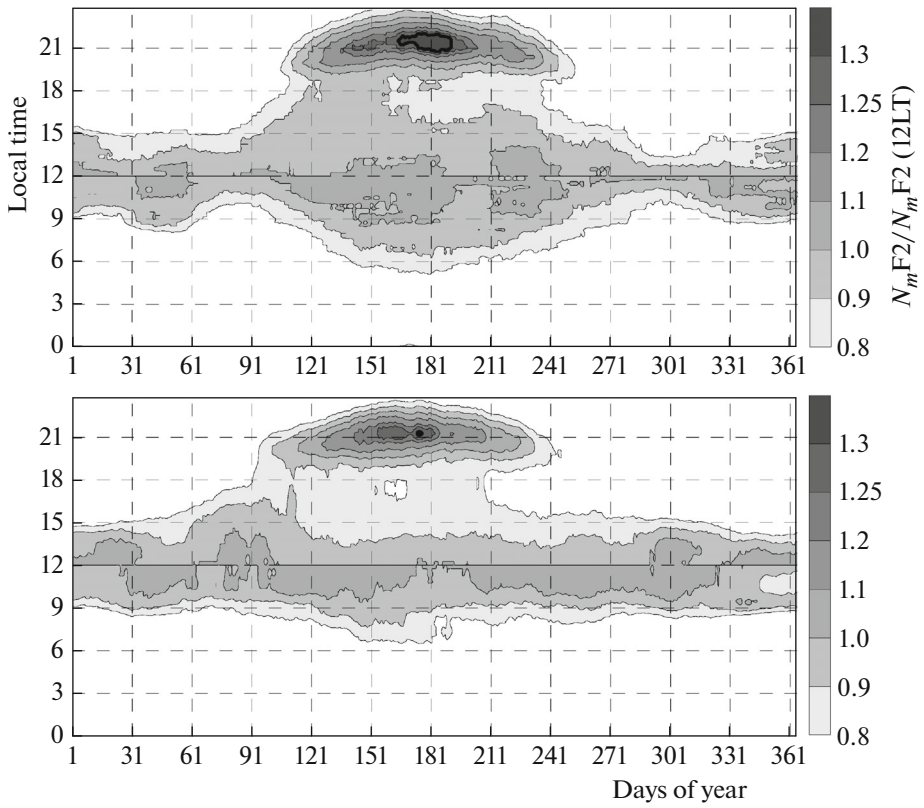

Fig. 2. Maps of the distribution of the N_mF2(LT, DOY)/N_m*F2*(12 LT, DOY) ratio, where N_mF2(LT, DOY) and N_mF2(12 LT, DOY) are the 27-day moving median values of the electron density in the maximum of the F2 ionospheric layer N_mF2 obtained for the day with number DOY at a local time LT and at 12 LT, respectively, drawn in the DOY–LT coordinates by using data from the Irkutsk (52° N, 104° E) (top) and Kaliningrad (54° N, 20° E) (bottom) ionosondes collected in 2009.

in the longitudinal variations at the medium and subauroral latitudes. Note also that, in the middle latitudes of the northern hemisphere, the longitudinal variation is less noticeable.

The latter fact is confirmed by Fig. 2, which shows the diurnal variations of the electron density normalized by the midday values at the maximum of the F2 layer, N_mF2, at the minimum of the solar activity (2009) for all seasons as measured with ionosondes in Irkutsk (52° N, 104° E) and Kaliningrad (54 ° N, 20° E). This figure was obtained as follows. Based on the values of N_mF2 measured with the Irkutsk and Kaliningrad ionosondes, the 27-day moving median values of N_mF2 (LT, DOY; LT is the local time, DOY is day of year) were calculated. Thereafter, the ratio of NmF2 to its midday value, N_mF2(LT, DOY)/N_mF2(12 LT, DOY), was calculated. This ratio was used as an indicator of the formation of the summer dusk peak. It is seen that the diurnal variations at these stations only slightly differ from each other. The most distinct difference is that this ratio for the summer dusk peak over Irkutsk is greater more than for that over Kaliningrad. According to [37], the longitudinal variation in the summer northern hemisphere is most evident the Yakutsk (subauroral analogue Irkutsk) and St. Petersburg (subauroral analogue Kaliningrad) stations. Thus, a comparison our results with those from [37] confirmed the conclusion we have drawn above based on IC-19 satellite observations: the longitudinal variation in the northern hemisphere at the subauroral latitudes is much stronger than at the mid-latitudes.

3. THE RESULTS OF CALCULATIONS USING THE GSM TIP

To theoretically interpret the longitudinal variations in the electron density, we performed numerical simulation within the framework of the GSM TIP [27, 28], modified regarding the description of electric fields of ionospheric and magnetospheric origins, [29]. The GSM TIP was developed at the Laboratory of Modeling of Ionospheric Processes of the Western Branch of the IZMIRAN. It is based the numerical integration of a system of quasi-hydrodynamic equations of continuity, momentum, and heat balance for the neutral and charged species of the near-Earth multicomponent cold plasma, consisting of O_2, N_2, O, NO, N(^2D), N(^4S), molecular ions (O_2^+, NO^+, N_2^+) atomic ions (O^+, H^+), and electrons, along with the equation for the electric potential in the range of altitudes from 80 km to a geo-

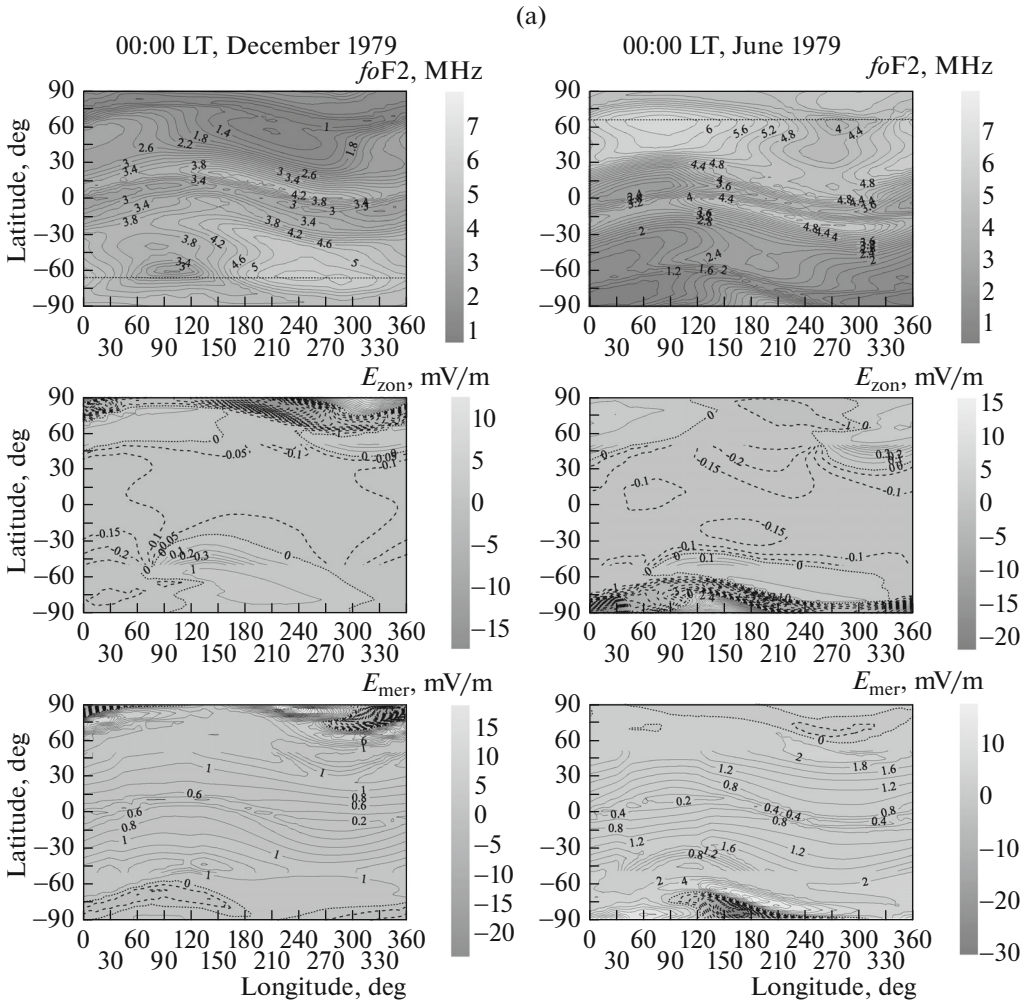

Fig. 3. (a) Nighttime longitudinal variations of the critical frequency *fo*F2 of the F2 layer, zonal components of the electric field E_{zon} (positive toward the east), and meridional component of the electric field E_{mer} (positive toward the equator) at an altitude of 300 km calculated by the GSM TIP for December (left) and June (right) 1979. The horizontal dashed line in the *fo*F2 map shows the position of the solar terminator. (b) The nighttime longitudinal variations of the neutral gas temperature T_n, molecular nitrogen concentration $n(N_2)$, atomic oxygen-to-molecular nitrogen concentration ratio $n(O)/n(N_2)$, and meridional component of the thermospheric wind $V_{n,mer}$ (positive in the direction from the North to the South Pole) at an altitude of 300 km as calculated by the GSM TIP for December (left) and June (right) 1979.

centric distance of 15 Earth's radii with allowance for the offset between the geographic and geomagnetic axes. Distinctive features of the GSM TIP were discussed in the introduction. It should be noted that, in the GSM TIP, the Earth's magnetic field is approximated by a central dipole, which makes it impossible to reproduce the difference between the longitudinal variations in the southern and northern hemispheres that arises due to the different distances between the geographic and geomagnetic poles in the two hemispheres [35]. To investigate longitudinal variations in quiet geomagnetic conditions, we performed calculations for the conditions of the summer and winter solstices (22.06.1979 and 12.22.1979) at a high solar activity without regard for thermospheric tides at the lower boundary (80 km) of the GSM TIP.

Figure 3 displays maps of *fo*F2, zonal and meridional components of the electric field, neutral temperature, concentration of molecular nitrogen $n(N_2)$, ratio of the concentrations of atomic oxygen of molecular nitrogen $n(O)/n(N_2)$, and meridional component of the thermospheric wind at an altitude of 300 km, calculated by the GSM TIP for December and June 1979. A comparison of the *fo*F2 maps with each other shows that the nighttime longitudinal variation of *fo*F2 in the summer hemisphere is greater than that in the winter hemisphere. The main longitudinal features are nighttime maxima: at a latitude of 65° S and longitudes of 220° E–300° E in the summer southern hemisphere in December 1979 and at a latitude of 65° N and longitudes of 35° E–120° E in the summer northern hemisphere in June 1979. These peaks are associated with

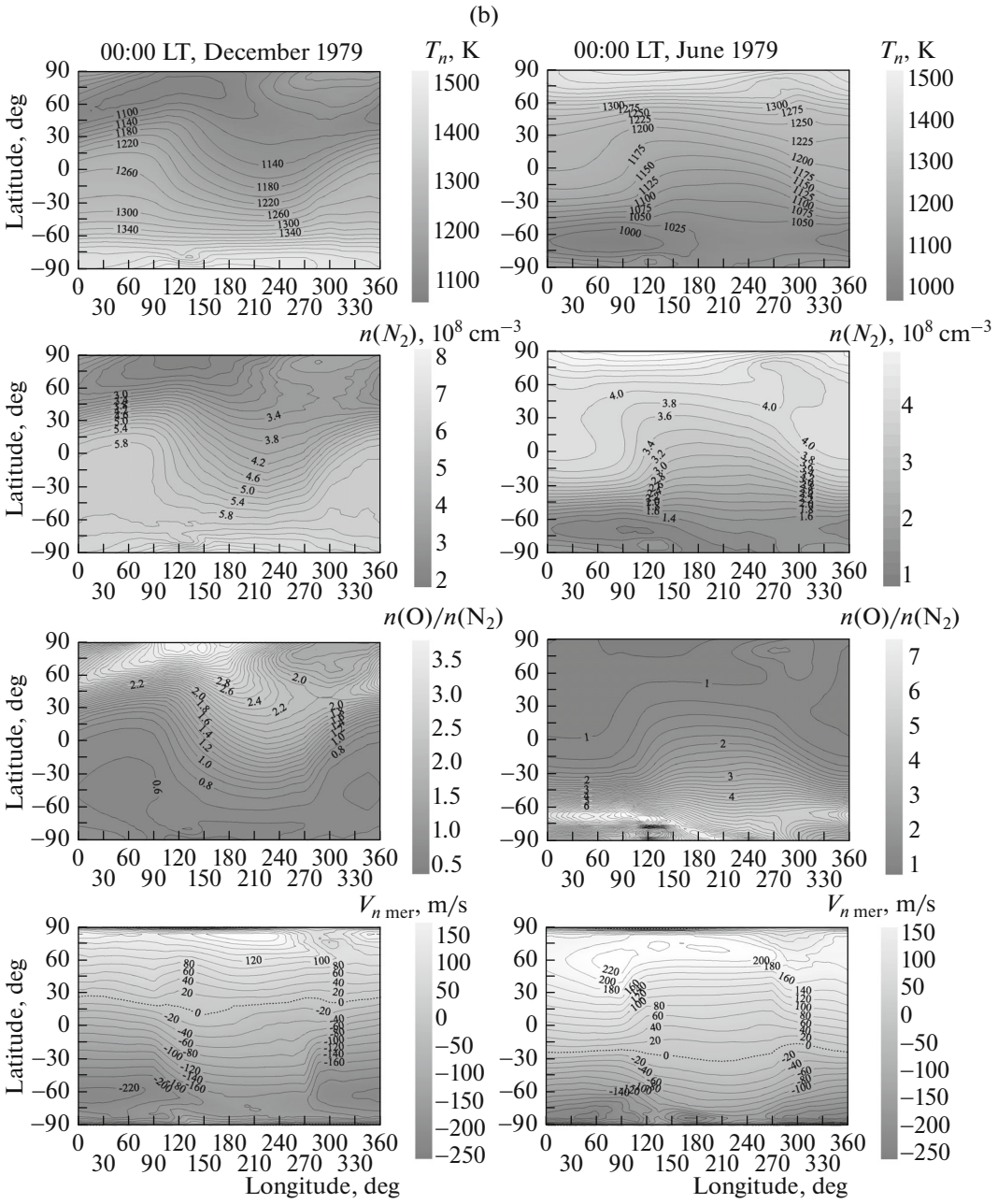

Fig. 3. (Contd.).

the Weddell Sea and the Yakutsk subauroral anomalies, which are characterized by an excess of the nighttime values of *fo*F2 over in the daytime values in the diurnal variation of *fo*F2. Note that the summer polar caps (all longitudes and latitudes from 65° S to the South Pole in December and from 65° N to the North Pole in June) are illuminated round-the-clock by the sun, which is confirmed by the solar terminator line shown on these maps. However, it is seen that *fo*F2 maxima are formed both in the illuminated part, on one side from the terminator line, and in the unilluminated part, on the other side from the line terminator. The reason for the formation of a maximum in the *fo*F2 distribution in the illuminated part, in the presence of solar radiation, can be somehow understood. However, the formation of a maximum in the unilluminated part, in the absence of solar radiation, requires explanation. To do this, let us examine in more detail the maps shown in Fig. 3.

The distribution of the zonal component of the electric field (Fig. 3a), causing the electromagnetic drift in the geomagnetic meridian plane upwards to the pole at the eastern field and downwards to the equator at the western field, shows that, in the winter in the

southern (summer) hemisphere, at longitudes of 300° E–360° E, the drift is directed from the pole to the equator, i.e., from the illuminated cap to the unilluminated region of lower latitudes. At longitudes of 120° E–300° E, the direction of the drift is opposite, i.e., from the unilluminated auroral region to the illuminated polar cap. The distribution of the meridional component of the electric field (Fig. 3a), which causes the electromagnetic drift in the eastward direction at the field directed to the equator and in the westward direction at the field directed to the pole, demonstrates that, in the winter in the southern (summer) hemisphere at longitudes of 220° E–360° E, the drift is directed westward, whereas at lower longitudes, eastward. Thus, in the Weddell Sea anomaly region, the electromagnetic drift of plasma is directed clockwise, transferring plasma with a higher density from the illuminated polar cap to the anomaly, thereby helping to create here a *fo*F2 maximum. The same occurs in the summer northern hemisphere in the Yakutsk anomaly region, but in this case, the drift of plasma is directed counterclockwise, transferring high-density plasma from the illuminated polar cap to the Yakutsk anomaly, thereby helping to create a *fo*F2 maximum.

An analysis the maps displayed in Fig. 3b reveals a heat-up in the longitudinal variation of the neutral gas temperature at the latitude of the Weddell Sea in the winter and at the latitude of the Yakutsk anomaly in the summer. This heat-up leads to an increase in the concentration of molecular nitrogen and to a decrease in the $n(O)/n(N_2)$ ratio in the anomalies, i.e., the enhancement in the rate of loss, a factor that hampers the formation of a *fo*F2 maximum in the region of the anomalies. At the same time, in the regions of the Weddell Sea and Yakutsk anomalies, this heat-up gives rise to a maximum in the nighttime variation of the meridional component of the thermospheric wind directed toward the equator. Due to ion–neutral collisions, the wind toward the equator transfers plasma along the geomagnetic field lines upward, to the region with lower rates of chemical loss, thereby causing an increase in *fo*F2.

Thus, we have demonstrated that peaks in the nighttime longitudinal distribution of *fo*F2 in the Weddell Sea anomaly in the winter in the southern (summer) hemisphere and in the Yakutsk anomaly in the summer in the northern (summer) hemisphere are formed by horizontal plasma drifts in the F regions of the ionosphere and by the thermosphere wind toward the equator if the polar cap is illuminated. In this case, the longitudinal variations of $n(N_2)$ and $n(O)/n(N_2)$ hamper the formation of these peaks.

In the winter hemisphere, the main ionospheric trough is observed not only in the nighttime, but also at the illuminated side, whereas in the summer hemisphere, only in the nighttime. The main ionospheric trough exists at all longitudes. As for longitudinal variations of the main ionospheric trough formed in the winter hemisphere during the solstice periods, Fig. 3*a* shows that the longitudinal variations are mainly related to the longitudinal variations of the electric field. In this case, changes in the thermospheric wind (Fig. 3b) have little effect on the longitudinal variations of the trough, whereas the longitudinal variations of $n(N_2)$ and $n(O)/n(N_2)$ (Fig. 3b) lead mainly to a decrease in the depth of the trough.

The night longitudinal variations of the EA in our model calculations do not feature the longitudinal effect of known structure with four harmonics, but show only one maximum in the longitudinal distribution of *fo*F2 at low latitudes. This is because our calculations do not take into account thermospheric tides at the lower boundary of the GSM TIP, while these tides, as stated in [38], are responsible for the formation of the four-harmonics structure of ionospheric longitudinal variations in the EA region. Thus, the longitudinal effect in our calculations is associated only with the offset between the geographic and geomagnetic axes. This means that, in the dipole approximation of the geomagnetic field, this offset yields only one harmonic in the longitudinal distribution of the electron density in the ionosphere at both middle and low latitudes.

Since the calculations by the GSM TIP (Fig. 3) ignored thermospheric tides at the lower boundary of the model (80 km), the longitudinal variations at low latitudes and geomagnetic equator have a distinct connection only with the geomagnetic field, as evidenced by the behavior of *fo*F2 isolines parallel to dipole geomagnetic parallels. To show the effect of thermospheric tides on the nighttime longitudinal variations of the ionosphere, we performed calculations within the framework of the GSM TIP for the conditions of the winter solstice at the minimum of solar activity with and without account of thermospheric tides at the lower boundary of the model. Figure 4 displays maps of the nighttime longitudinal variations of the zonal electric fields at an altitude of 300 km and the critical frequency *fo*F2 of the F2 layer for December 2009. The maps of the zonal component of the electric field shows that the inclusion of thermospheric tides leads to a significant change in the zonal component of the electric field at low latitudes and equator due to the generation of a dynamo field in the conductive layer of the ionosphere by thermospheric tides. It is evident a noticeable longitudinal variation of the electric field arises, which manifests itself in the longitudinal variation of the equatorial anomaly in *fo*F2. As a result, while in the absence of thermospheric tides, nothing except the connection of the longitudinal variation with the geomagnetic field in the equatorial anomaly region is seen, in the presence of thermospheric tides, a well-pronounced three-wave structure in the longitudinal variation of the *fo*F2 equatorial anomaly arises, which is consistent with IC-19 observations for the maximum of solar activity.

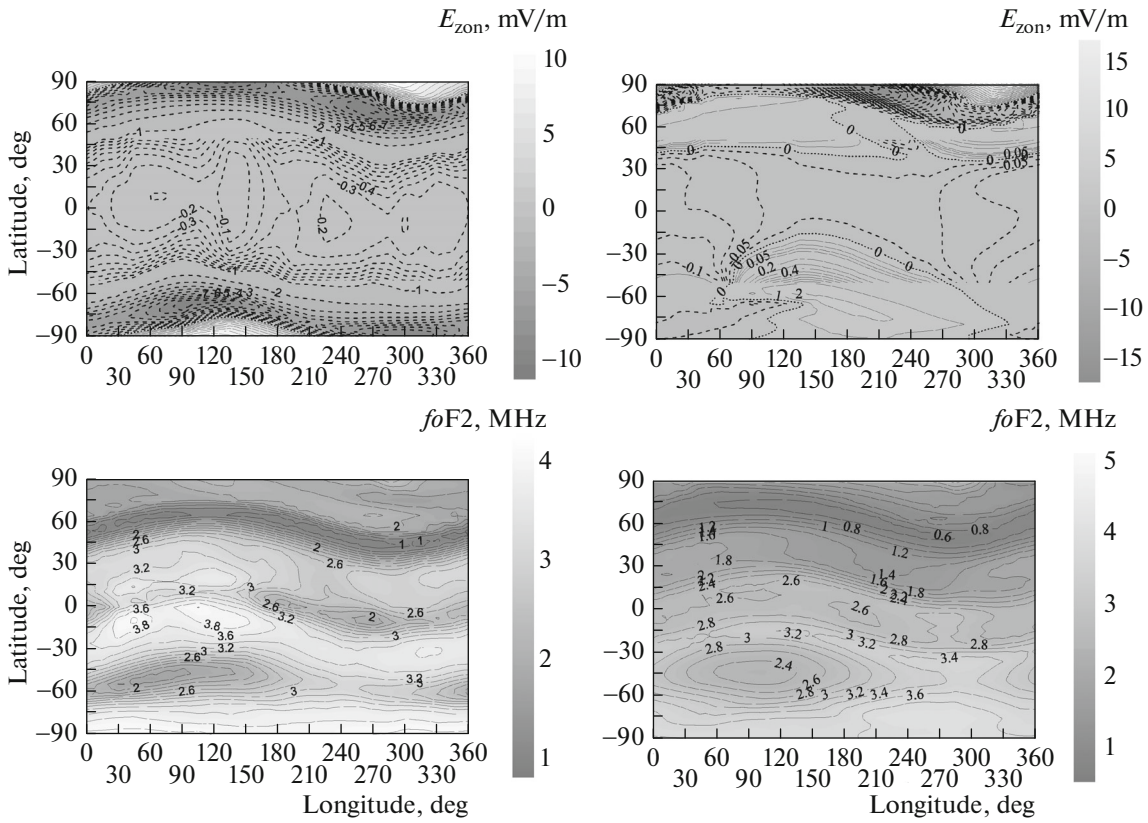

Fig. 4. Nighttime longitudinal variations of the zonal electric field E_{zon} (positive toward the east) at an altitude of 300 km (above) and of the critical frequency *fo*F2 of the F2 layer (below) at 00:00 LT December 2009 calculated with (left) and without (right) account of tides on the lower boundary (80 km) of the GSM TIP.

Thus, the results of simulations using the GSM TIP are indicative of significant differences in the formation of longitudinal variations at different latitudes. For example, longitudinal variations in the equatorial anomaly region are produced by the distribution of the dynamo electric field, which is determined by thermospheric tides. At high and subauroral latitudes, the electric field also plays a major role in the formation of the longitudinal variation in these areas. However, in this case, it is formed by the horizontal rather than vertical transfer of plasma. For the middle latitudes, the main mechanism of the formation of longitudinal variations is the thermospheric wind, which carries plasma vertically along the lines of the geomagnetic field.

4. CONCLUSIONS

Based on a vast body of data obtained from the IC-19 satellite and the Irkutsk and Kaliningrad ionosonde measurements, we studied the morphological features of longitudinal variations of the electron density and the critical frequency at the maximum of the F region of the ionosphere at various latitudes. Calculations within the framework of the GSM TIP qualitatively reproduce the observational data from the IC-19 satellite, which makes it possible to answer the question about the main reasons and the physical mechanisms of the formation of the observed longitudinal variations in the ionosphere at the middle latitudes. The mechanisms of the formation of the Yakutsk anomaly and Weddell Sea anomaly are the same, with the main one being the geometric factor of superposition of the action of the thermospheric wind, heating and ionization of the neutral atmosphere by solar radiation, and horizontal transfer due to electromagnetic drift. The longitudinal variations of *fo*F2 at different latitudes, although related, arise via substantially different mechanisms. For instance, at high latitudes, the leading role in the formation of longitudinal variations is played by electromagnetic drift, in the mid-latitudes, by the vertical transfer of plasma under the action of thermospheric wind, and in the low latitudes by vertical electromagnetic drift.

ACKNOWLEDGMENTS

This work was supported by the Russian Foundation for Basic Research, project nos. 14-05-00788 and 15-35-20364. The studies were conducted within the

project "Physical Mechanisms of the Formation of the Response of Upper Atmosphere and Ionosphere to Processes in the Lower Atmosphere and on the Earth's Surface" (the task the Ministry of Education and Science of the Russian Federation, competition part, state contract no. 3.1127.2014/K).

REFERENCES

1. M. G. Deminov and A. T. Karpachev, Geomagn. Aeron. **26**, 63 (1986a).
2. M. G. Deminov and A. T. Karpachev, Geomagn. Aeron. **26**, 682 (1986b).
3. W. H. Bellchambers and W. R. Piggott, Nature **182**, 1596 (1958).
4. A. P. Mamrukov, Geomagn. Aeron. **21**, 984 (1971).
5. I. Horvath, J. Geophys. Res. A **111**, 12317 (2006). doi: 10.1029/2006JA011679
6. I. Horvath and B. C. Lovell, J. Geophys. Res. A **114**, 02306 (2009). doi: 10.1029/2008JA013719
7. C. H. Lin, J. Y. Liu, C. Z. Cheng, et al., J. Geophys. Res. A **114**, 02312 (2009). doi: 10.1029/2008JA013455
8. M. G. Deminov and A. T. Karpachev, Geomagn. Aeron. **26**, 63 (1986).
9. M. G. Deminov and A. T. Karpachev, Geomagn. Aeron. **26**, 682 (1986).
10. N. A. Kochenova, Geomagn. Aeron. **27**, 142 (1987).
11. M. G. Deminov and A. T. Karpachev, Geomagn. Aeron. **27**, 76 (1987).
12. A. T. Karpachev, Geomagn. Aeron. **28**, 46 (1988).
13. A. T. Karpachev, Geomagn. Aeron. **28**, 620 (1988).
14. V. V. Afonin, M. G. Deminov, and A. T. Karpachev, Geomagn. Aeron. **32** (2), 75 (1992).
15. G. F. Deminova, Geomagn. Aeron. **33** (5), 167 (1993).
16. N. A. Kochenova and V. N. Shubin, Geomagn. Aeron. **35** (2), 155 (1995).
17. G. F. Deminova, Geomagn. Aeron. **42**, 736 (2002).
18. G. F. Deminova, Adv. Space Res. **31**, 531 (2003).
19. V. S. Mingalev, V. N. Krivilev, M. L. Yevlashina, and G. I. Mingaleva, Pure Appl. Geophys. (PAGEOPH) **127**, 323 (1988).
20. V. M. Uvarov, P. D. Barashkov, and A. P. Zakharova, Geomagn. Aeron. **32** (3), 70 (1992).
21. A. V. Pavlov, Ann. Geophys. **21**, 1601 (2003).
22. A. V. Tashchilin and E. B. Romanova, Mat. Model. **25** (1), 3 (2013).
23. R. W. Schunk, Pure Appl. Geophys. (PAGEOPH) **127**, 255 (1988).
24. G. J. Bailey, N. Balan, and Y. Z. Su, J. Atmosph. Sol.-Terr. Phys. **59**, 1541 (1997). doi: 10.1016/S1364-6826(96)00155-1
25. J. D. Huba, G. Joyce, and J. A. Fedder, J. Geophys. Res. **105**, 23035 (2000).
26. J. D. Huba, G. Joyce, and J. Krall, Geophys. Rev. Lett. **35**, L10102 (2008). doi: 10.1029/2008GL033509
27. A. A. Namgaladze, Yu. N. Korenkov, V. V. Klimenko, et al., Pure Appl. Geophys. (PAGEOPH) **127**, 219 (1988).
28. Y. N. Korenkov, V. V. Klimenko, M. Förster, F. S. Bessarab, and V. A. Surotkin, J. Geophys. Res. A **103**, 14697 (1998). doi: 10.1029/98JA00210
29. M. V. Klimenko, V. V. Klimenko, and V. V. Bryukhanov, Geomagn. Aeron. **46**, 457 (2006).
30. A. A. Namgaladze, O. V. Martynenko, and A. N. Namgaladze, Geomagn. Aeron. **36**, 207 (1996).
31. A. D. Richmond, E. C. Ridley, and R. G. Roble, Geophys. Rev. Lett. **6**, 601 (1992).
32. G. H. Millward, I. C. F. Muller-Wodrag, A. D. Aylward, et al., J. Geophys. Res. **106**, 24733 (2001). doi: 10.1029/2000JA000342
33. A. T. Karpachev, M. V. Klimenko, V. V. Klimenko, G. A. Zhbankov, and V. A. Telegin, J. Atmosph. Sol.-Terr. Phys. **77**, 186 (2012). doi: 10.1016/j.jastp.2011.12.018
34. M. V. Klimenko, V. V. Klimenko, and A. T. Karpachev, J. Atmosph. Sol.-Terr. Phys. **90–91**, 179 (2012). doi: 10.1016/j.jastp.2012.02.011
35. V. V. Klimenko, A. T. Karpachev, and M. V. Klimenko, Russ. J. Phys. Chem. B **7**, 611 (2013). doi: 10.7868/S0207401X13090070
36. C. H. Lin, C. H. Liu, J. Y. Liu, A. G. Burns, and W. Wang, J. Geophys. Res. A **115**, 03308 (2010). doi: 10.1029/2009JA014084
37. O. M. Pirog, N. M. Polekh, and L. V. Chistyakova, Adv. Space Res. **27**, 1395 (2001).
38. J. Oberheide, J. M. Forbes, X. Zhang, and S. L. Bruinsma, J. Geophys. Res. A **116**, 01306 (2011). doi: 10.1029/ 2010JA015911

Translated by V. Smirnov